Acta Oceanol. Sin., 2020, Vol. 39, No. 11, P. 91–102
https://doi.org/10.1007/s13131-020-1678-x
http://www.hyxb.org.cn
E-mail: hyxbe@263.net

Statistical analysis of mesoscale eddy propagation velocity in the South China Sea deep basin

Runqi Huang[1], Lingling Xie[1, 2*], Quanan Zheng[3], Mingming Li[1, 2], Peng Bai[1, 2], Keyi Tan[1]

[1] Laboratory of Coastal Ocean Variation and Disaster Prediction, College of Ocean and Meteorology, Guangdong Ocean University, Zhanjiang 524088, China

[2] Marine Resources Big Data Center of South China Sea, Southern Marine Science and Engineering Guangdong Laboratory (Zhanjiang), Zhanjiang 524025, China

[3] Department of Atmospheric and Oceanic Science, University of Maryland, College Park, Maryland 20742, USA

Received 15 June 2020; accepted 10 August 2020

Abstract

Using mesoscale eddy trajectory product derived from satellite altimetry data from 1993 to 2017, this study analyzes the statistical characteristics of spatiotemporal distribution of mesoscale eddy propagation velocities ($\boldsymbol{C}$) in the South China Sea (SCS) deep basin with depths >1 000 m. Climatologically, the zonal propagation velocities (c_x) are westwards in the whole basin, and the meridional velocities (c_y) are southwards in the northwestern basin, and northwards in the southeastern basin. The variation of c_y with longitude is consistent with that of the background meridional currents with correlation coefficient R^2 of 0.96, while the variation of c_x is related both to the background zonal currents and β effect. The propagation velocities characterize significant seasonality with the minimum magnitude occurring in summer and the maximum in winter for c_x and $\boldsymbol{C}$. Interannually, larger values of c_x and c_y mostly occurred in La Niña years in the negative phase of the Pacific Decadal Oscillation (PDO). Mesoscale eddies move fast at the beginning and end of their life span, i.e., at their growth and dissipation periods, and slowly during their stable "midlife" period. This trend is negatively correlated with the rotating tangential velocity with R^2 of –0.93. Eddies with extreme propagation velocities are defined, which are slower (faster) than 1.5 cm/s (15.4 cm/s) and take 1.5% (1.9%) of the total eddies. The extremely slow-moving (fast-moving) eddies tend to appear in the middle (on the edge) of the basin, and mostly occur in summer (winter). The mechanism analysis reveals that the spatiotemporal distributions of the propagation velocities of mesoscale eddies in the SCS are modulated by the basin-scale background circulation.

Key words: South China Sea, mesoscale eddies, eddy propagation velocity, variation in life span, eddies with abnormal speeds

Citation: Huang Runqi, Xie Lingling, Zheng Quanan, Li Mingming, Bai Peng, Tan Keyi. 2020. Statistical analysis of mesoscale eddy propagation velocity in the South China Sea deep basin. Acta Oceanologica Sinica, 39(11): 91–102, doi: 10.1007/s13131-020-1678-x

1 Introduction

Mesoscale eddies broadly distributed in the global oceans are one of the primary processes responsible for marine material and energy transports (Chelton et al., 2011; Adams et al., 2011; Hausmann and Czaja, 2012; Zhang et al., 2014, 2016; Yang et al., 2015; He et al., 2018; Zhang and Guan, 2019). Therefore, they play important roles in global climate change, ocean circulation, marine ecological environment, and fishery distribution. Mesoscale eddies directly affect the three-dimensional distribution of deep-sea sediments and ecological-environmental factors such as concentrations/distributions of chlorophyll and nutrients (Lobel and Robinson, 1986; Salihoğlu et al., 1990; McGillicuddy et al., 1998; Johnson et al., 2005; Benitez-Nelson et al., 2007; Adams et al., 2011; Frenger et al., 2018). The propagation velocity of mesoscale eddy, i.e., $\boldsymbol{C}$ (bold indicates vector), directly determines the fluxes of material and energy transports. It is thus important to explore the temporal and spatial distribution characteristics and variations of the eddy propagation velocities (Morrow et al., 2004; Cheng and Qi, 2008; Yang et al., 2013; Pilo et al., 2015; Lü et al., 2017).

The South China Sea (SCS) is a large marginal sea in the Northwest Pacific, where mesoscale eddies are very active due to disturbances from the Pacific, seasonally reversed monsoons, and the complex bottom topography (Xie et al., 2016; Xie and Zheng, 2017; Zheng et al., 2017, 2019). Previous researchers have used satellite observations and numerical simulations to statistically characterize mesoscale eddies in the SCS in terms of scale, intensity, numbers, and structure (Wang et al., 2003, 2005; Lin, 2005; Zheng et al., 2007, 2011, 2014; Chen et al., 2011; Li et al., 2011; Lin et al., 2012a; Cui, 2015; Huang et al., 2016; He et al., 2018). Mesoscale eddies in the SCS are mainly distributed in areas where depths exceed 1 000 m and there is an approximately equal probability of occurrence of cyclonic (CE) and anticyclonic eddies (AE) (Zheng et al., 2017). As reviewed by Zheng et

Foundation item: The National Natural Science Foundation of China under contract Nos 41776034 and 41706025; the Fund of Southern Marine Science and Engineering Guangdong Laboratory (Zhanjiang) under contract No. ZJW-2019-08; the Special Project of Global Change and Air and Sea Interaction under contract No. GASI-02-SCS-YGST2-02; the Guangdong Province First-Class Discipline Plan under contract Nos CYL231419012 and 231389002; the Scientific Research Setup Fund of Guangdong Ocean University under contract No.101302/R18001.

*Corresponding author, E-mail: xiell@gdou.edu.cn

al. (2017), the eddies have an average life span of 8.8 weeks, an average surface radius of 132 km and a maximum rotating tangential velocity of ⩽40 cm/s, with the radius and rotating tangential velocity typically decreasing with increasing depth. Previous researchers have also studied the seasonal and interannual variations of the eddy numbers and the eddy kinetic energy (EKE) in the SCS (Chen, 2010; Chu et al., 2017; Xiu et al., 2010; Tuo et al., 2019). They found more CEs (AEs) occur in summer (winter), and more eddies and larger EKE occurred in La Niña years.

General characteristics of the propagation velocity of mesoscale eddies in the SCS have been determined by previous researchers. For instance, Wang et al. (2003) analyzed multi-satellite sea surface height anomaly (SSHA) data of 1993–2000, and found that the maximum propagation velocity of mesoscale eddies, i.e., $|\boldsymbol{C}|$ occurred in the southwest of the Luzon Island, followed by those northwest of Luzon Island, while the minimum velocity occurred near Vietnam coast. Lin (2005) analyzed SSHA data from 1992 to 2002 and found that >80% of mesoscale eddies in the SCS propagated westward during this period. In addition, they determined the latitudinal distribution characteristics of mesoscale eddy zonal propagation velocities. Chen et al. (2011) used altimeter data from 1992 to 2009 to characterize SCS mesoscale eddies, and determined the 17-year averaged vector field of $\boldsymbol{C}$. They found the eddies propagate southwestward along the continental slope at a velocity of 5.0–9.0 cm/s, and quasi-westward at 2.0–6.4 cm/s in the central SCS.

Zheng et al. (2017) reviewed the progress in mesoscale eddies in the SCS over the past 60 years including the general horizontal propagation patterns of mesoscale eddies similar to that in Chen et al. (2011). Recently, He et al. (2018) re-evaluated the mesoscale eddies in the SCS using the SSH data from 1993 to 2015, and found that the westward-propagating CEs deflect southward while the AEs deflect northward in the western SCS. In addition, previous researchers have also examined the characteristics of $\boldsymbol{C}$ in local areas, such as that southwest of Taiwan, the Luzon Strait, and the Dongsha Islands (Nan et al., 2011; Lin et al., 2012b; Chow et al., 2008; Shu et al., 2016, 2019). Among these, the propagation velocity reaching 9.3 cm/s were observed in southwestward background flow in the northern SCS (Chow et al., 2008). Wu and Chiang (2007) indicated that mesoscale eddies have the same propagation speed as baroclinic Rossby waves by using fine-grid resolution model. Xie et al. (2018) used Rossby normal mode theory to analyze the characteristics of the propagation velocities of grouped mesoscale eddies in the SCS basin. They found the westward propagation velocities of the first three baroclinic modes are about 2–4 cm/s. Shu et al. (2019) found the eddy propagation decreased near island due to interaction of eddy and topography. These results imply that complicated variability and mechanism for the eddy propagation in the SCS.

In summary, previous researchers have determined the multi-year average spatial distribution characteristics of the propagation velocities of mesoscale eddies in the SCS, but a systematic understanding of the temporal and spatial variations of $\boldsymbol{C}$, and the governing mechanisms is lacking. Thus, we herein use statistical methods to analyze the spatial and temporal distribution of the propagation velocities of mesoscale eddies in the SCS, elucidate their seasonal, interannual, and life cycle variations, and explore the mechanisms that affect their spatiotemporal distribution characteristics.

2 Data and methods

2.1 *Data sources*

This study uses two datasets, i.e., the archiving validation and interpretation of satellite data in oceanography (AVISO) mesoscale eddy trajectory data and the simple ocean data assimilation (SODA v3.7.2) ocean current data. Time series of Niño3.4 index and PDO index are also used.

The AVISO mesoscale eddy trajectory data are the product of eddies identified and tracked based on multi-satellite altimetry data (Chelton and Schlax, 2011). The dataset includes tracking days, the amplitude, type, rotating tangential velocity (V_e), and radius of eddies, as well as the longitudes and latitudes of the eddy centers. The data span the period from January 1, 1993 to January 6, 2017 with a time resolution of one day.

The SODA data include the global ocean current data from 1980 to 2015 with a spatial resolution of 0.5° × 0.5°. This study uses the monthly-mean surface current velocity as the background current velocities ($\boldsymbol{V}$, with two components u, v).

2.2 *Data processing*

The study area comprises the deep basin area of the SCS with depths >1 000 m as shown in Fig. 1. The mesoscale eddy trajectory data are used to calculate propagation velocities $\boldsymbol{C}$ with the methods detailed below.

The center locations (longitude x and latitude y) of the same eddy (numbered n) on two successive days (t) is used to calculate the zonal and meridional components of the eddy propagation velocity, i.e., zonal propagation velocity c_x and meridional propagation velocity c_y, respectively. Then, the instantaneous propagation velocity vector $\boldsymbol{C}(x, y, t, n)$ of an eddy (numbered n) at the location (x, y) on the day (t) is obtained. For each eddy, there is a one-to-one correspondence between the location x, y and the time t in the life span. The averaged propagation velocity of an eddy numbered n, i.e., $\overline{C}^t(n)$, is the average of all instantaneous velocities in the whole life span, $^{-t}$ denotes average on dimension of t. The averaged propagation velocity at a fixed position x, y, i.e., $\overline{C}^n(x, y, t)$, is the average of the instantaneous velocities of all eddies passing through the position at time t.

3 Climatically spatial distribution characteristic

3.1 *Horizontal distribution*

We divide the study area into grids of 1°×1°, and then average the instantaneous zonal (meridional) propagation velocities of all eddies passing through the grid to obtain the climatological zonal (meridional) propagation velocity $\overline{c_x}^{n,t}(x_i, y_j)$ (eastward positive) ($\overline{c_y}^{n,t}(x_i, y_j)$, northward positive) in each grid (x_i, y_j). The results are shown in Figs 1a and b. Then, the zonal and meridional components are combined to obtain the propagation velocity vectors $\overline{C}^{n,t}(x_i, y_j)$ as shown in Fig. 1c.

From Fig. 1a, one can see that $\overline{c_x}^{n,t}$ is westward in the whole basin of the SCS. It is faster in the northern and southern slope of the SCS at 8–10 cm/s, but slower at 0–2 cm/s in the central SCS and areas near Vietnam. For the meridional velocities (Fig. 1b), $\overline{c_y}^{n,t}$ has opposite directions within the basin, i.e., southward in the northern and western sides, but northward in the southern and eastern sides. $\overline{c_y}^{n,t}$ has the highest values of 3–5 cm/s at the boundaries, while that in the central basin are the lowest, measuring 0–2 cm/s.

For the total velocities $\overline{C}^{n,t}$ (Fig. 1c), the results are similar to the previous results (Zheng et al., 2017), of which mesoscale eddies propagate southwestward along the continental slope at a velocity of 8–11 cm/s in the northern SCS, westward at velocities of 2–5 cm/s in the central basin, and westward or northwestward at 6–12 cm/s in the southern basin.

The distribution characteristics of the propagation velocities

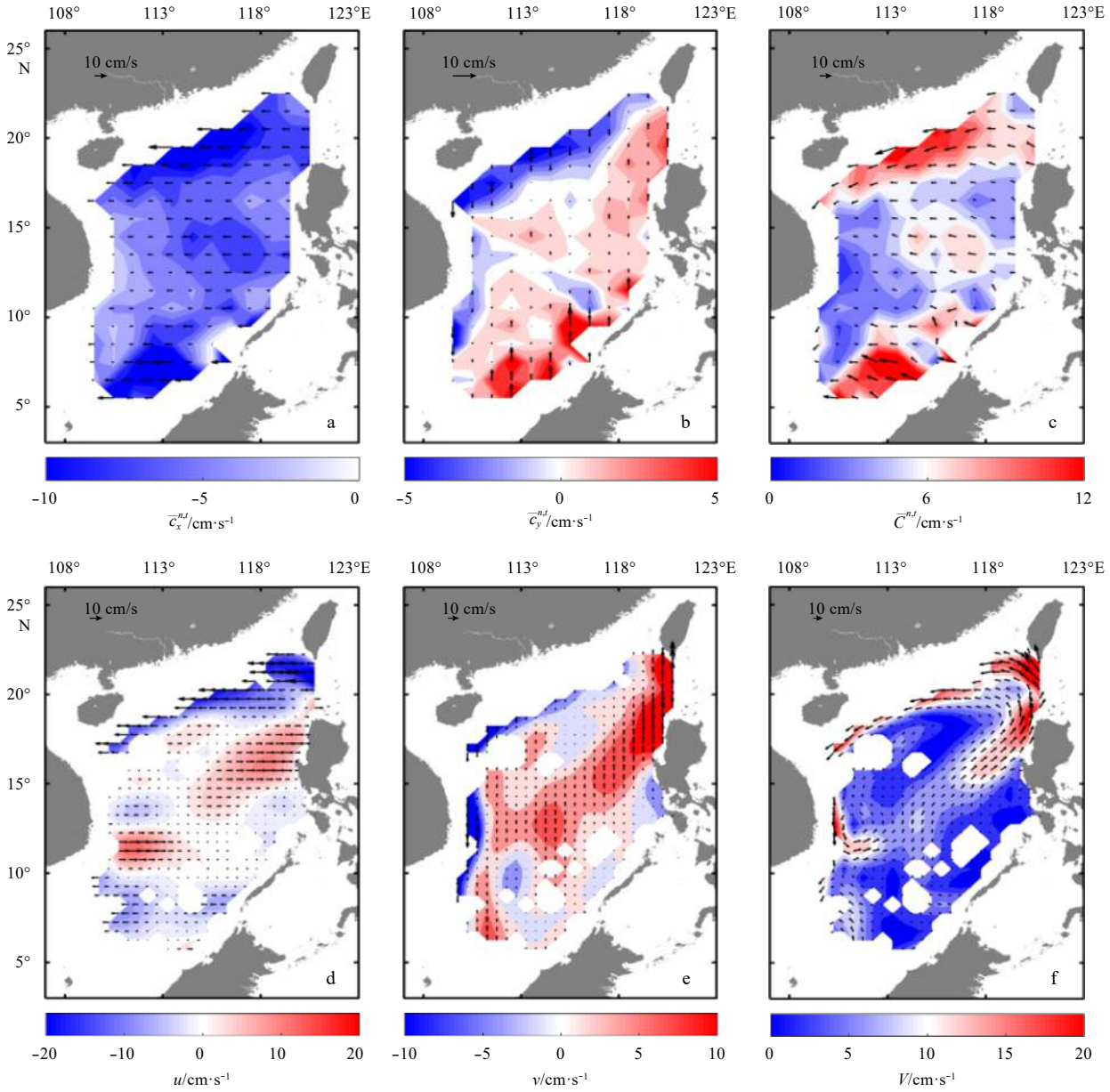

Fig. 1. Climatological distribution of zonal ($\overline{c_x}^{n,t}$, a), meridional ($\overline{c_y}^{n,t}$, b) and total ($\overline{C}^{n,t}$, c) propagation velocities of mesoscale eddies in the SCS, and the corresponding zonal (u, d), meridional (v, e), and total (V, f) velocities of the background current. Color codes and arrows represent the velocity magnitudes and directions, respectively. Minus values mean westward for c_x and u, and southward for c_y and v.

of cyclones and anticyclones are generally consistent with the overall eddy characteristics outlined above, and not shown here.

3.2 *Meridional and zonal variation*

We zonally average the propagation velocities to obtain their meridional variation. As shown in Fig. 2a, the mean zonal velocity $\overline{c_x}^{n,t,x}$ is westward at all latitudes, with higher values of 6–9 cm/s at 17°–22°N and 4°–7°N, and lower values of 3–4 cm/s in the central basin at 8°–12°N. The mean meridional velocity $\overline{c_y}^{n,t,x}$ has opposite directions in the north and south of 15°N (Fig. 2b). It is generally within a range of ±1 cm/s, much smaller than $\overline{c_x}^{n,t,x}$. $\overline{C}^{n,t,x}$ is thus dominated by $\overline{c_x}^{n,t,x}$ and has a general "Σ" shape with latitudes, i.e., first decreases and then increases as the latitude decreses (Fig. 2c).

For the meridional average, $\overline{c_x}^{n,t,y}$ has smaller values of 3–5 cm/s in west of 111°E (Fig. 3a), where $\overline{c_y}^{n,t,y}$ has largest southward values of 3.5 cm/s (Fig. 3b). In the central basin, $\overline{c_x}^{n,t,y}$ has values larger than 5 cm/s, while $\overline{c_y}^{n,t,y}$ is quite smaller than 1 cm/s. In the east of 118°E, $\overline{c_y}^{n,t,y}$ is northward at 2–4 cm/s and $\overline{c_x}^{n,t,y}$ is westward at 4–6 cm/s. Thus, eddies have high total propagation velocities $\overline{C}^{n,t,y}$ above 4 cm/s at 112°–116°E (Fig. 3c). The increases in meridional component lead to an increased total propagation velocity in the eastern basin.

3.3 *Mechanism analysis*

Previous studies have shown that westward propagating mesoscale eddies are dominated by the beta effect and nonlinearity (Cheng et al., 2005), although the background current also affect these eddies directly (Zheng et al., 2017).

Since the geostrophic current from AVISO may affected by the

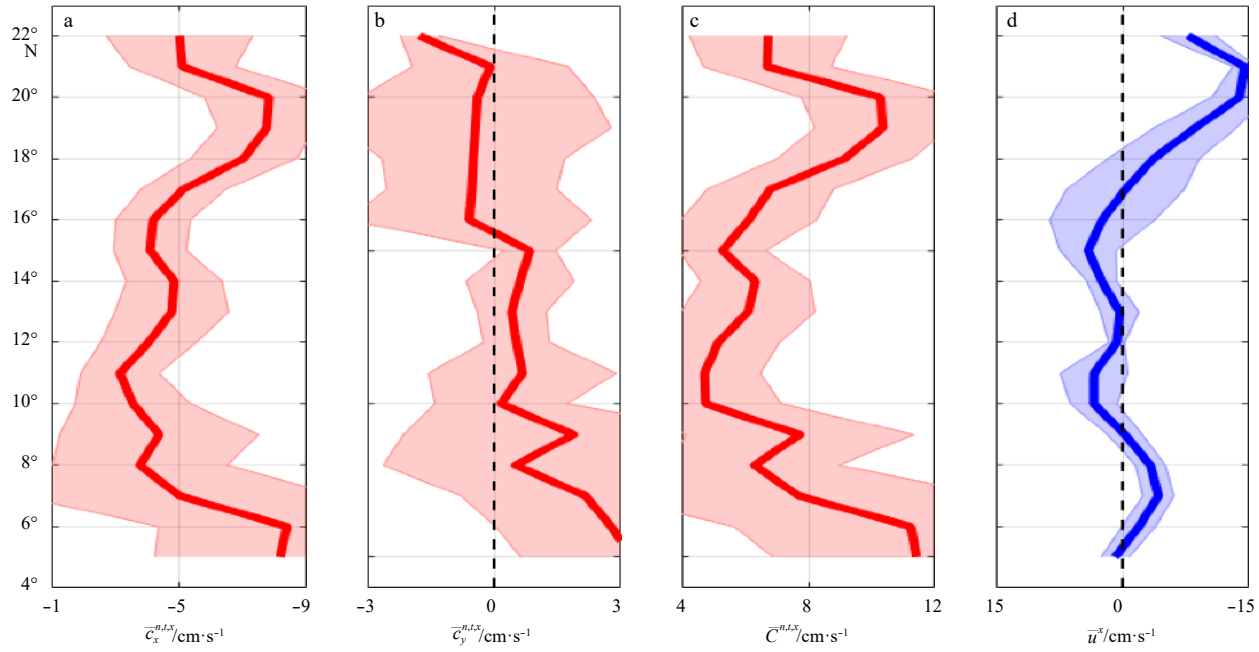

Fig. 2. Meridional distributions of zonal-mean zonal ($\overline{c_x}^{n,t,x}$, a), meridional ($\overline{c_y}^{n,t,x}$, b) and total ($\overline{C}^{n,t,x}$, c) propagation velocities of overall mesoscale eddies in the SCS and zonal velocity ($\overline{u}^{x}$, d) of the background current. Color shade represents standard deviation of the mean values. Minus values mean westward for c_x and u, and southward for c_y.

eddies themselves, we use the climatological mean surface velocities from the SODA data to represent the total background current in the upper ocean of the SCS. The results of background velocity components u, v and total velocity V are shown in Figs 1d–f. Similar to the eddy propagation velocities shown in Figs 1a–c, the background current flows southwestward along the northern slope, southward along the western boundary and recirculates northward along the eastern boundary with strong velocities larger than 15 cm/s. Qualitatively, the larger $\overline{c_x}^{n,t}$ in the northern slope are consistent with the larger u, and the southward and northward $\overline{c_y}^{n,t}$ in the western and eastern sides are consistent with v. It indicates that propagation velocity of mesoscale eddies is closely related to the velocity of background current. We calculate the correlation coefficient between the eddy propagation velocities and the background current velocity. The results are 0.34 and 0.49 with significant level of both 99% for zonal and meridional components, respectively.

We further calculate the zonal-mean zonal background current velocities $\overline{u}^{x}(y)$, and the meridional-mean meridional background current velocities $\overline{v}^{y}(x)$, as shown in Figs 2d and 3d, respectively. The correlation coefficient between $\overline{c_x}^{n,t,x}$ and $\overline{u}^{x}(y)$ and that between $\overline{c_x}^{n,t,x}$ and $\overline{v}^{y}(x)$ are 0.46 and 0.96, with significant level higher than 95% and 99%, respectively. It indicates that the meridional eddy propagation is dominantly affected by the background meridional current, while the zonal propagation velocities depends both on background current and other effects. The larger β at low latitudes may contribute to larger $\overline{c_x}^{n,t,x}$ in the south. However, the β variation cannot explain the increasing $\overline{c_x}^{n,t,x}$ in the norther basin, where the increasing westward $\overline{u}^{x}(y)$ should play important role.

4 Characteristics of temporal variation

4.1 *Seasonal variation*

4.1.1 *Monthly distribution*

Figures 4a and b show the monthly distribution of the zonal and the meridional propagation velocities in the SCS, respectively. The ratio of the number of westward (northward) propagating eddies ($N_{W,}$ N_N) to that of eastward (southward) propagating ones ($N_{E,}$ N_s), i.e., N_E/N_W (N_N/N_S) are also shown as green lines. The eddies mostly propagate westward with N_E/N_W less than 0.3. The mean westward propagation velocity $\overline{c_{xW}}^{n,x,y}(t)$ changes from 6.8 cm/s in winter to 5.1 cm/s in summer (blue bars), while $\overline{c_{xE}}^{n,x,y}(t)$ are in range of 3.7–4.4 cm/s (red bars) with less seasonal variation. N_E/N_W gets larger in months of June–August, indicting eastward-moving eddies increase in summer. On the other hand, northward and southward propagation velocities ($\overline{c_{yN}}^{n,x,y}(t)$ and $\overline{c_{yS}}^{n,x,y}(t)$) have almost equal magnitudes of 4–5 cm/s and the ratio of eddy numbers (N_N/N_S) is near 1. The monthly variation of $\overline{c_{yN}}^{n,x,y}$ and $\overline{c_{yS}}^{n,x,y}$ is not evident.

Figure 5a shows the monthly distribution of average zonal propagation velocities of all mesoscale eddies ($\overline{c_x}^{n,x,y}(t)$) in the SCS. $\overline{c_x}^{n,x,y}$ are averagely westward in each month since both $\overline{c_{xW}}^{n,x,y}(t)$ and N_w are larger than $\overline{c_{xE}}^{n,x,y}(t)$ and N_E. On average, $\overline{c_x}^{n,x,y}$ is the fastest in winter (December–February) at 6.0 cm/s, followed by that in spring (March–May) and autumn (September–November) (5.0 cm/s), with that in summer being the slowest (4.1 cm/s). In contrast, $\overline{c_y}^{n,x,y}$ (Fig. 5b) is within a range of relatively small values of ±0.4 cm/s for whole year, due to the offset of almost-equal northward and southward velocities. As for total propagation velocities (Fig. 5c), eddies have a maximum average velocity of 7.6 cm/s in winter and reaches a minimum of 6.3 cm/s in summer. The variation of total velocity follows the zonal components $\overline{c_x}$.

Cyclones and anticyclones exhibit similar seasonal variations in propagation velocities, but cyclones propagate faster than anticyclones in spring and autumn, while slower in summer and winter (not shown).

4.1.2 *Mechanism analysis*

As indicated in Section 3, the spacial variation of the eddy

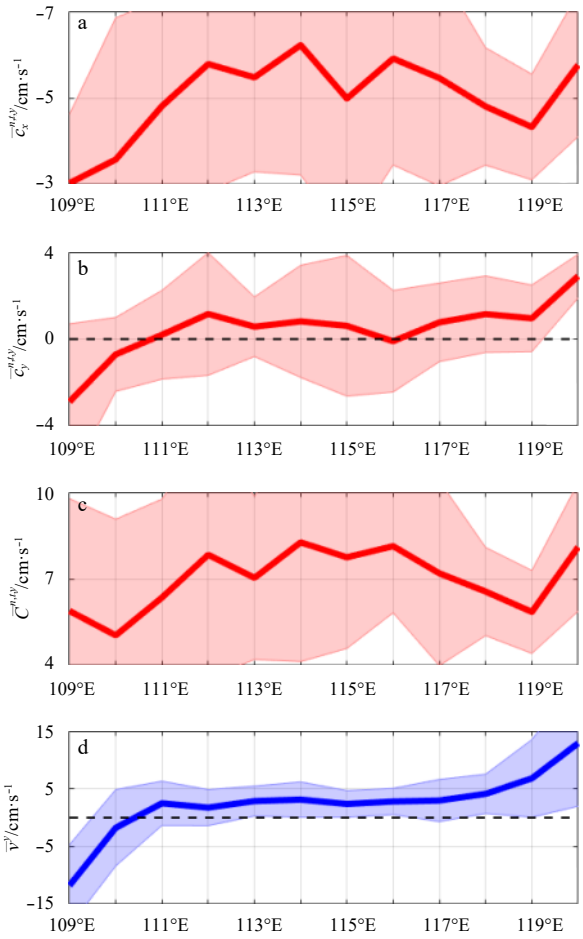

Fig. 3. Zonal distributions of meridional-averaged zonal ($\overline{c_x}^{n,t,y}$, a), meridional ($\overline{c_y}^{n,t,y}$, b) and total ($\overline{C}^{n,t,y}$, c) propagation velocities of mesoscale eddies in the SCS and meridional velocity ($\overline{v}^{y}$, d) of the background current. Color shade represents standard deviation of the mean values. Minus values mean westward for c_x and u, and southward for c_y.

propagation velocities is related to the variation of the background current. Here, for the temporal variation, we further investigate the seasonal variation of the upper ocean circulation in the SCS.

As has shown in many studies (Hu et al., 2000; Wang et al., 2019), there is a cyclonic circulation in the SCS basin in winter, driven by the northeasterly monsoon, and consistent with the southwestward moving velocities of the eddies. From June to August, when the summer southwesterly monsoon prevails, the basin circulation is bounded at 12°: in the north is a cyclonic circulation and in the south is an anticyclonic circulation, which is reverse to the eddy propagation velocities. This implies that the seasonal reversed ocean circulation is favorable to occurrence of the maximum and minimum eddy propagation velocities in winter and summer, respectively. Though Cheng et al. (2005) pointed out that the reversed monsoon direction is the reason, the seasonal-reversed upper ocean circulation may play more important and direct roles in the seasonal variability of the eddy propagation.

The monthly distribution of averaged background zonal, meridional and total velocities (u, v, V) are further shown in Figs 5a–c. Corresponding to the westward background velocity, the zonal eddy velocity c_x have larger westward values. The correlation coefficient between the monthly variations of u and c_x reaches 0.97 (with significant level higher than 95%), indicating the strong effect of background current on the zonal eddy propagation.

4.2 *Interannual variation*

Figure 6 shows a time series of the spatial-averaged eddy propagation velocities in the SCS from January 1993 to December 2016. One can see that the zonal propagation velocity ($\overline{c_x}^{x,y,n}(t)$) in Fig. 6a are all westward with magnitudes fluctuate between 4–7 cm/s in each year. The large magnitudes (>6 cm/s) occurred in winter of 1993, 1995, 2000, 2008, 2011 and 2014, of which the fastest velocity was in 2008. The meridional propagation velocity ($\overline{c_y}^{x,y,n}(t)$, Fig. 6b) fluctuates between southward 1 cm/s and northward 1.5 cm/s with most values are positive.

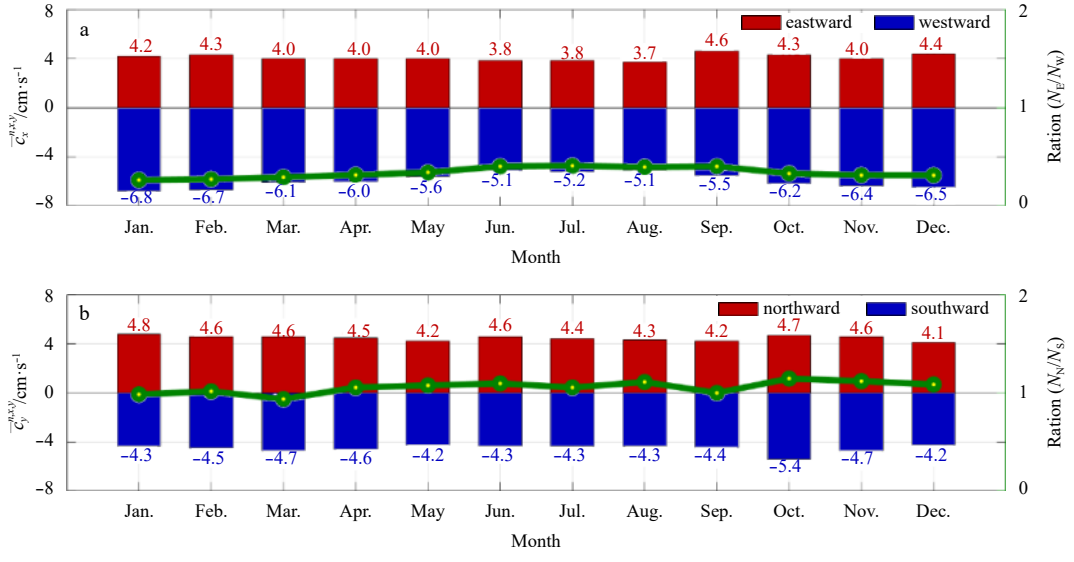

Fig. 4. Monthly distribution of mesoscale eddy propagation velocities in the SCS. Green lines represent the ratio of eddy numbers. Minus values mean westward for c_x, and southward for c_y.

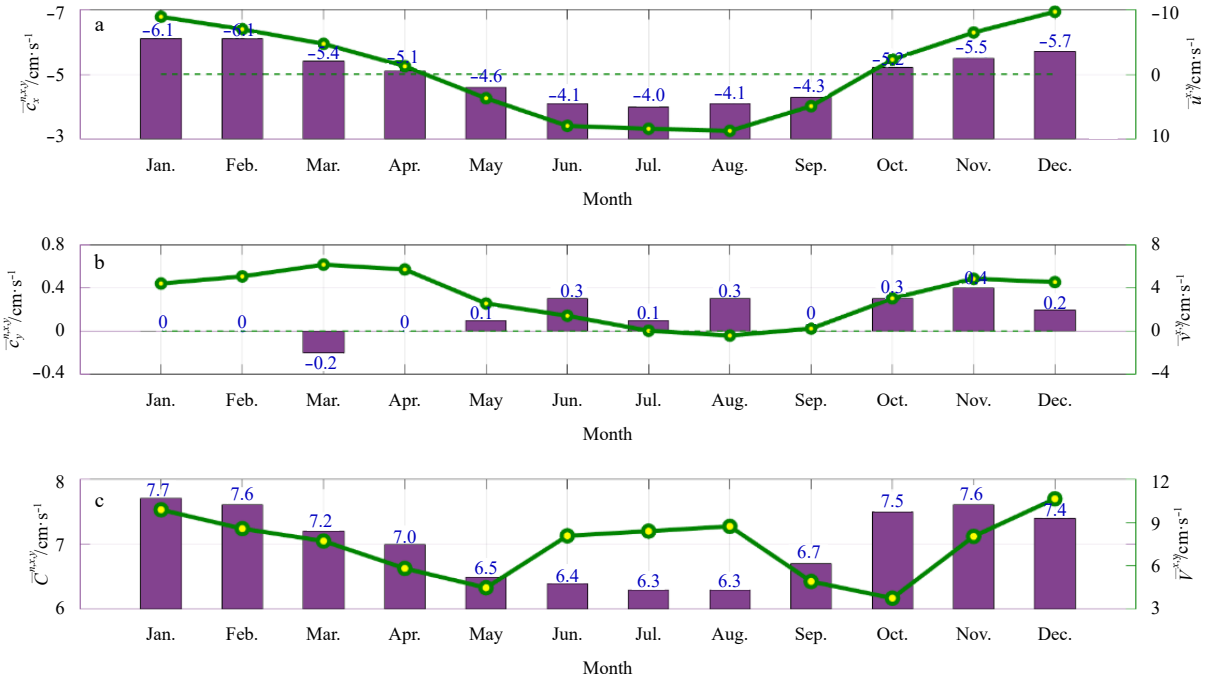

Fig. 5. Monthly distribution of the basin-averaged zonal ($\overline{c_x}^{n,x,y}$, a), meridional ($\overline{c_y}^{n,x,y}$, b), and total velocities ($\overline{C}^{n,x,y}$, c) of mesoscale eddies in the SCS. Green lines represent the monthly distribution of background current velocities $\overline{u}^{x,y}$, $\overline{v}^{x,y}$, and $\overline{V}^{x,y}$. Minus values mean westward for c_x, and southward for c_y.

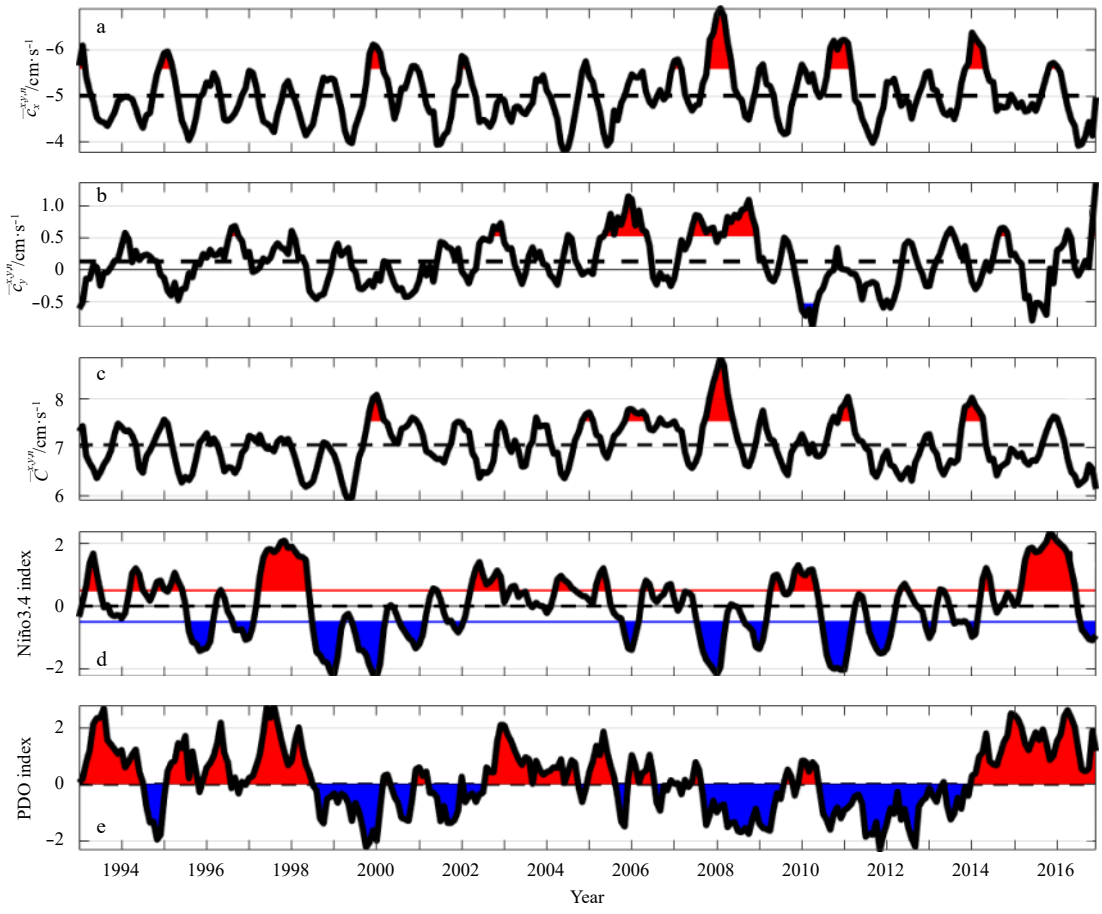

Fig. 6. Interannual variation of the mean zonal ($\overline{c_x}^{x,y,n}$, a), meridional ($\overline{c_y}^{x,y,n}$, b) and total ($\overline{C}^{x,y,n}$, c) propagation velocity of mesoscale eddies in the SCS from January 1993 to December 2016. Niño3.4 index and PDO index are shown in d and e, respectively. Minus values mean westward for c_x and u, and southward for c_y.

The northward $\overline{c_y}^{x,y,n}$ larger than 1 cm/s occurred in 2006, 2008–2009 and 2016, while the southward $\overline{c_y}^{x,y,n}$ larger than 0.5 m/s occurred in 2010 and 2015. The larger values of $\overline{c_x}^{x,y,n}$ and $\overline{c_y}^{x,y,n}$ mostly occurred in different years and different seasons if in the same year. The total propagation velocity $\overline{C}^{x,y,n}$ in Fig. 6c has larger values in 2000, 2006, 2008, and 2014, and smaller values in 1999.

Comparing the variations of propagation velocities to that of the Niño 3.4 index and the PDO index shown in Figs 6d and e, one can see that most of the larger zonal and meridional velocities occurred in La Niña years in the negative phase of PDO. The largest two-month lag correlation coefficients (R^2) of $\overline{c_x}^{x,y,n}$, $\overline{c_y}^{x,y,n}$ and $\overline{C}^{x,y,n}$ with the Niño3.4 index are 0.45, –0.04, and –0.39 with significant levels of 99%, 90% and 99%, respectively. For the PDO index, the correlation coefficients are 0.22, –0.03, and –0.19 with significant levels of 99%, 90% and 99%, respectively. It implies that the ENSO and PDO events play roles in the zonal propagation of the SCS eddies.

As analyzed in previous sections, the background circulation can directly affect the variation of the eddy propagation in the SCS. It has been widely reported that the ENSO and PDO events can affect the SCS circulation through the atmospheric and ocean and bridges (Qu et al., 2004; Wang et al., 2006; Cheng et al., 2016; Wei et al., 2019; Zu et al., 2020). The ENSO effects on specific eddy generation have also been reported (He et al., 2016; Chu et al., 2017; Tuo et al., 2019). Bao (2007) pointed out that the cyclonic circulation in the SCS weakened during the strong El Niño event in 1997–1998. In contrast, the cyclonic circulation in the SCS is expected to increase during the La Niña events. Thus, the eddy westward propagation speed increases as shown in Fig. 6. Qiu et al. (2015) found that there were easterly wind abnormal in the northern SCS during the negative phase period of PDO index, which could also increase the westward circulation in the SCS and thus the westward propagation of the eddies. That is to say, the ENSO and PDO events modulated the background wind and water circulations and then affect the eddy propagation in the SCS.

4.3 *Variation during the life span*

Figure 7 shows the averaged total propagation velocity $\overline{C}^n(t)$ (red curve) and rotating velocity $\overline{V_e}^n$ (blue curve) in the normalized eddy life span in the SCS. One can see that mesoscale eddies propagate rapidly with a maximum velocity of 8.5 cm/s at the beginning and ending of the life span, but slowly during the middle. On the other hand, $\overline{V_e}^n$ are lower at 26 cm/s at the beginning and the end, but higher above 31 cm/s in the middle. According the variation of the velocities, we divided the whole eddy life into three stages, i.e., the growth stage ($d\overline{C}^n/dt<0$; $d\overline{V_e}^n/dt>0$), the stable stage ($d\overline{C}^n/dt\sim0$; $d\overline{V_e}^n/dt\sim0$) and the dissipation stage ($d\overline{C}^n/dt>0$; $d\overline{V_e}^n/dt<0$), which takes the first 20%, the middle 50% and the last 30% of the eddy life span, respectively. In the growth stage, $\overline{C}^n$ gradually slows down, while $\overline{V_e}^n$ increases. In the stable stage, $\overline{C}^n$ and $\overline{V_e}^n$ stabilize to 7.0–7.2 cm/s and 31.0–31.5 cm/s, respectively. When the eddies reach 70% of their life span, $\overline{C}^n$ reaches a minimum of 6.7 cm/s. Then, $\overline{C}^n$ begins to accelerate (while $\overline{V_e}^n$ gradually decreases), continuing to do so until the eddies dissipate.

From the above analysis, we find that $\overline{C}^n$ has a significant decrease-stable-increase variation in the three stages of the life span. In fact, such variation has been indicated by previous statistics in He et al. (2018, Fig. 6c), though they did not emphasize it. Liu et al. (2012) reported the life-span variation of the eddy kinetic energy (EKE), which is related to $\overline{V_e}^n$, in the North Pacific subtropical zone. They also found three stages, of which the stable stage takes 60% of the life span, and the dissipation stage is in the final 20%, later than the last 30% in the SCS. It seems that mesoscale eddies in the SCS decay earlier than those in the North Pacific. We further investigated the life-span variations of eddy propagation velocities in marginal seas such as the Japan Sea and the Andaman Sea. Similar results are derived (not shown), indicating the general three-stage variation pattern of eddy propagation velocities in the life span.

The analysis above also shows that the life-span variations of $\overline{C}^n$ and $\overline{V_e}^n$ are reversed. There is a strong correlation between an eddy propagation velocity and its rotating velocity during its life span. This is confirmed by the correlation coefficient of the two parameters as high as –0.93 with significant level of 99%. It is the first time to show clear correlation between the moving and rotating speeds of the mesoscale eddies. It seems that the moving energy convert to the rotating energy at the growth stage, and reverses at the dissipation stage. Considering the effects of background circulation on the propagation velocities and the eddy generation mechanism associated the barotropic and baroclinic

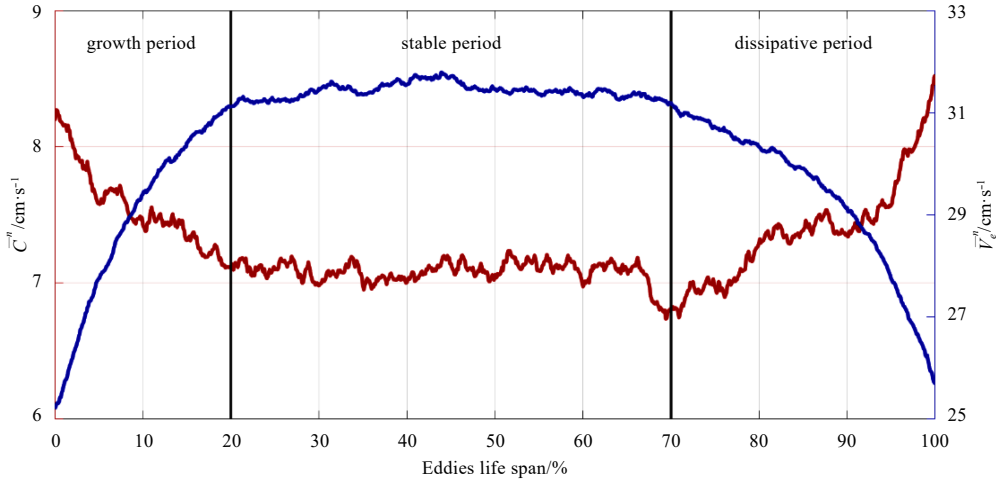

Fig. 7. Variation of the mean eddy propagation velocity ($\overline{C}^n$, red line) and rotating tangential velocity ($\overline{V_e}^n$, blue line) in the SCS during a normalized eddy life span.

instability, there might be positive energy cascade from the large-scale background current to mesoscale eddy, decreasing the propagation velocity and increasing the rotating velocity at the early growing stage, and the eddy energy transfer reverses to larger scale current at the dissipation stage.

5 Extreme velocity and its formation mechanism

5.1 *Spatial distribution*

Figures 8a and b show the spatial distributions of extremely slow-moving and extremely fast-moving eddies from 1993 to 2016. In this context, $|\boldsymbol{C}|$< 1.5 cm/s (bottom 5% of all propagation velocities) that are sustained for five days or more during the life span are denoted extremely slow-moving eddies (SMEs), while $|\boldsymbol{C}|$>15.4 cm/s (top 5% of all propagation velocities) that are sustained for 5 d or more are denoted as extremely fast-moving eddies (FMEs). There are 777 SMEs, accounting for 1.5% of the total number of eddies, and 976 FMEs, accounting for 1.9% of the total number of eddies. These SMEs and FMEs are mostly anticyclonic, accounting for 52.12% and 56.05% of the total, respectively.

As shown in Fig. 8, most of the SMEs (82.63%) occur in the central basin (10°–18°N), with only a small proportion appearing on the west side of the Luzon Strait. There are no SMEs south of 10°N. Most FMEs (68.55%) occur at the edge of the basin, especially in the northern and southern SCS, with only a small proportion (31.45%) appearing in the central basin.

Comparing with the background current shown in Figs 1d–f, the distribution of SMEs corresponds to the area with slow background current, reversely, the area containing FMEs has a fast background current. This implies that spatial distribution of SMEs and FMEs is closely related to the background current.

5.2 *Temporal variation*

5.2.1 *Seasonal distribution*

As shown in Fig. 9a, most of the SMEs occur in late spring and early summer. The SME numbers in May–July are twice higher than that in other months. For the spatial distribution, the SMEs mostly occur in the weak westward or eastward current in the central basin in winter, spring, and autumn, and shift toward the northern SCS as the eastward current in the anticyclonic circulation develops in summer.

Contrary to the SMEs, the FMEs mostly occur in winter (Fig. 9b), and are distributed at the northern and southern boundaries of the basin, where there are strong southwestward or northwestward currents (Figs 9g–j). As the weakening of the southwestward current in the northern SCS in spring, the number of FMEs decreases, and reaches a minimum in summer when anticyclonic circulation develops. FMEs are seldom found in the central basin where there are northeastward flow. In the autumn, FMEs increase again as cyclonic circulation strengthens.

The consistence of the variation of SMEs with the eastward current and the FMEs with westward current further indicate the effects of background circulation on the eddy propagation. The interaction of the current and eddies may further affect the mass transport and local biological processes.

5.2.2 *Interannual distribution*

We further investigate the distribution of SMEs and FMEs

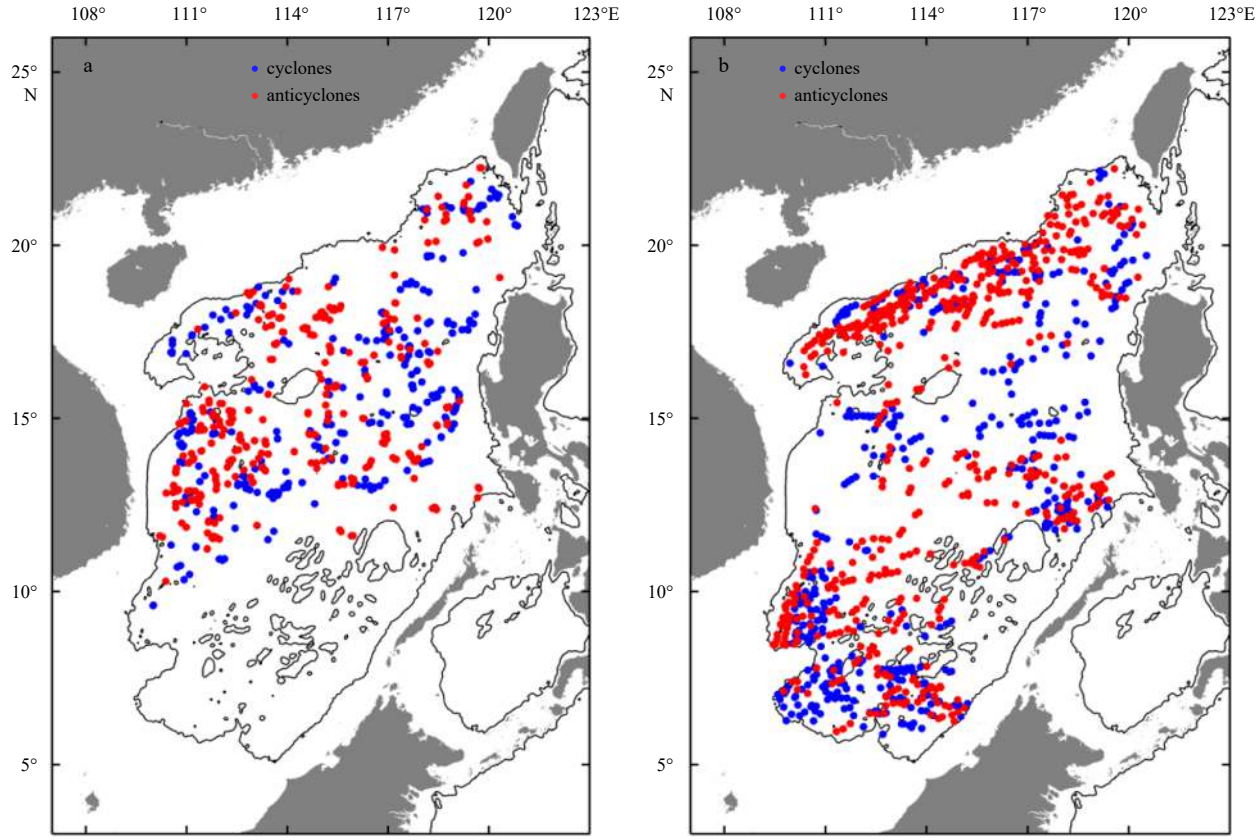

Fig. 8. Spatial distribution of extremely slow-moving (SMEs, a) and fast-moving (FMEs, b) eddies. Blue and red circles represent CEs and AEs, respectively. Black lines are the isobaths of 1 000 m.

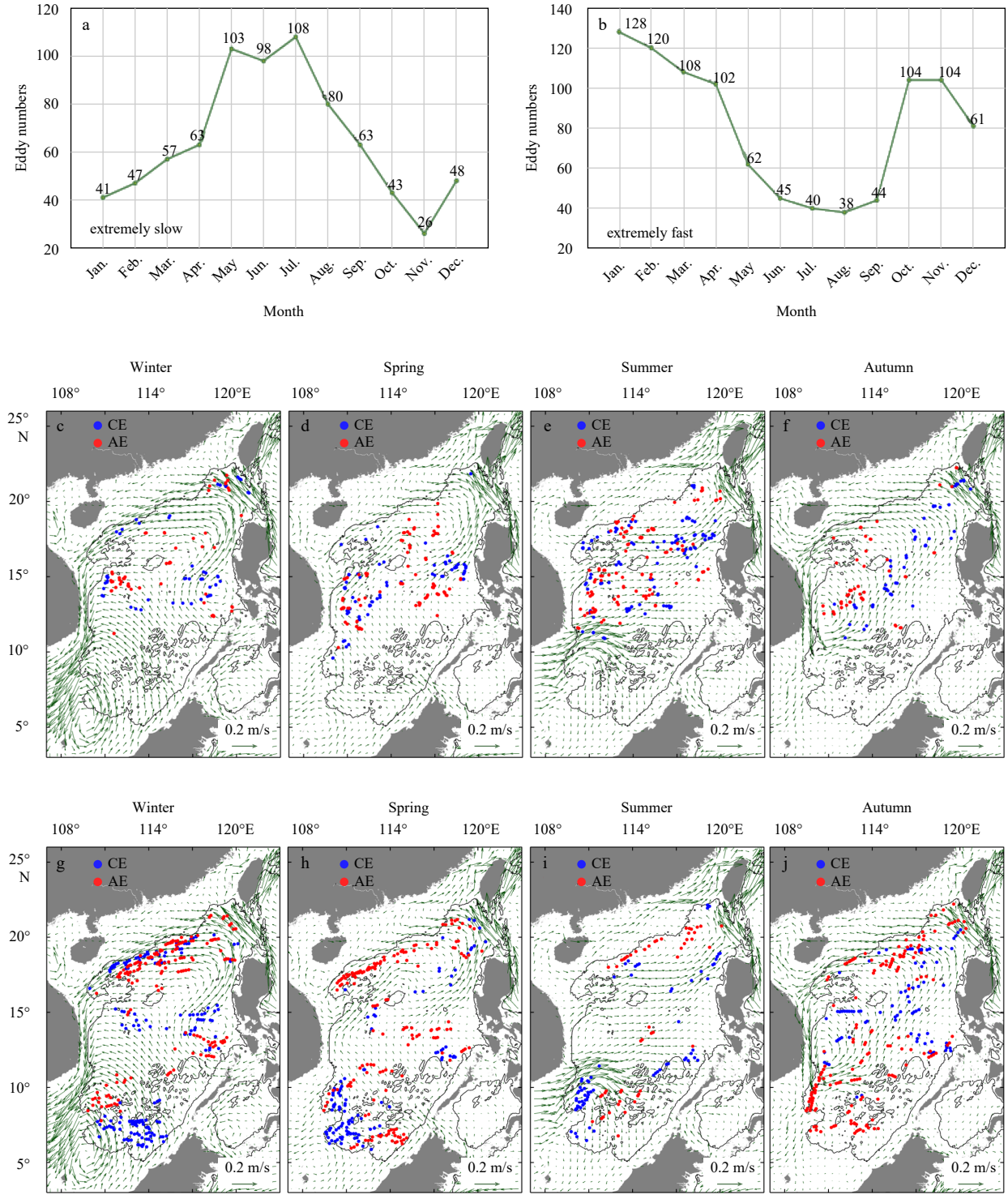

Fig. 9. Monthly distribution of the number of extremely slow-moving (SMEs, a) and extremely fast-moving (FMEs, b) eddies, and the spatial distribution of SMEs (c–f) and FMEs (g–j) in winter, spring, summer, and autumn. Arrows represent the background current.

during the El Niño and the La Niña events (Fig. 10). One can see that without reference to the El Niño and the La Niña events, the number of extremely slow-moving and fast-moving eddies fluctuates between 10–70 in each year. During the El Niño event, extremely slow-moving and fast-moving eddies are mainly anticyclonic (75.29% and 52.42%, respectively), while during the La Niña events, extremely slow-moving eddies are mostly cyclonic (56.73%), and extremely fast-moving eddies are mostly anticyclonic (57.89%).

6 Discussion

As reviewed in Section 1, previous investigators have shown eddy characteristics including eddy number, radius, and amplitudes in the SCS (i.e., Zheng et al., 2017). Though eddy propagation was partially involved in previous studies, the detailed spatiotemporal variation and mechanisms of the propagation velocit-

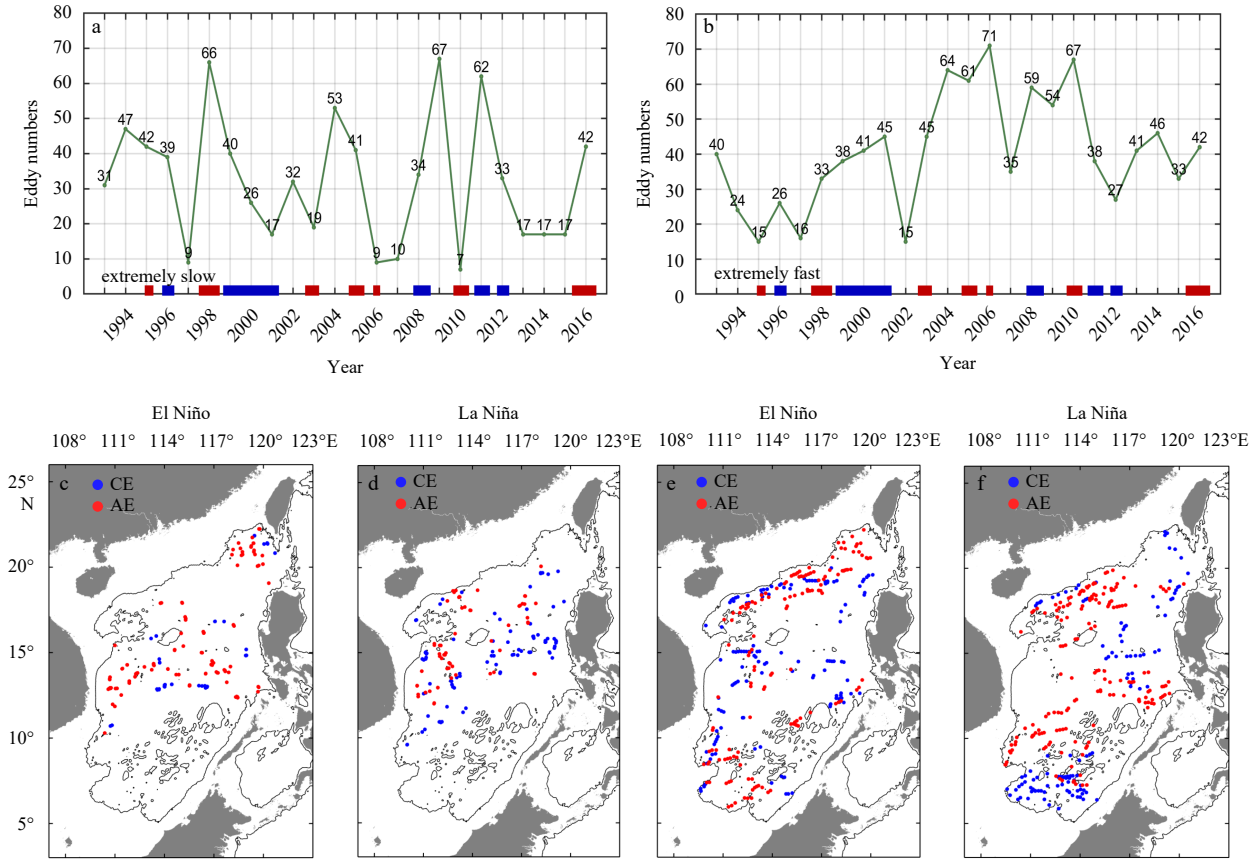

Fig. 10. Interannual variations of the numbers of SMEs (a) and FMEs (b), and their spatial distributions during the El Niño events (c and e) and the La Niña events (d and f). Red shade of the coordinate denotes values during El Niño and blue points that during La Niña.

ies is still lack of knowledge. Table 1 lists some of the previous studies involving the eddy propagation in the SCS. The presented magnitudes and directions of total velocities are generally consistent with our climatological results, while the variations of the zonal and meridional components are seldom focused on. In addition, we investigate the seasonal and interannual variations, find the high correlation between translation and rotating motions in the life span, and emphasize the effects of large-scale circulation on the eddy propagation.

7 Conclusions

This study uses satellite altimeter eddy trajectory data from

Table 1. Mesoscale eddy propagation velocities in previous studies

Ocean area	Data or method	Reference	Characteristics
SCS	SSHA from 1993 to 2000	Wang et al. (2003)	maximum propagation velocity in the southwest of the Luzon Island, while the minimum near Vietnam coast
SCS	SLA from 1992 to 2002	Lin (2005)	>80% of mesoscale eddies propagated westward and c_x in range of –8 cm/s to 3 cm/s
Northern SCS	fine-grid resolution model	Wu and Chiang (2007)	mesoscale eddies have the same propagation speed as the baroclinic Rossby waves
South or southwest of Dongsha Island	SLA from 2000 to 2005	Chow et al. (2008)	cyclonic eddy with propagation speed of about 9 cm/s
SCS	altimeter data from 1992 to 2009	Chen et al. (2011)	climatological map of propagate speed: southwestward in the northern SCS (5–9 cm/s), generally westward in the central basin (2–6 cm/s), westward or southwestward in the south (2–8 cm/s).
Southwest of Taiwan	altimeter data from 1992 to 2009	Nan et al. (2011)	most ACEs propagate westward, and CEs are often spun up to the east of the ACEs
Near the Luzon Strait	MSLA from 1993 to 2008	Lin et al. (2012b)	mesoscale eddies accelerate when passing through the Luzon Strait
Northern SCS	SLA from February to July 2015	Shu et al. (2016)	an anticyclonic eddy with translation velocity of about 5.2 cm/s
SCS basin	Rossby normal mode theory	Xie et al. (2018)	westward propagation of grouped eddies at about 2–4 cm/s
SCS	SSH from 1993 to 2015	He et al. (2018)	seasonal map of total propagation speed: higher in winter and slower in summer

1993 to 2017 to statistically analyze the spatial and temporal distributions of propagation velocity of mesoscale eddies in the SCS. The mechanism of the variation of the propagation velocities are discussed and associated with the background circulation. The new findings are summarized as follows.

(1) The zonal propagation velocities c_x are westward in the basin with higher values of 6–9 cm/s both in the north and south sides, while the weak meridional propagation velocities c_y (mostly less than 3.5 cm/s) are southward on the north and west sides, and oppositely northward on the south and east sides. The variation of c_y is highly related with the background meridional currents with correlation coefficient R^2 reaching 0.96, while the variation of c_x is related both to the zonal currents with R^2 of 0.46, and the beta effect.

(2) Seasonally, mesoscale eddies propagate slowest in summer (June–August) and fastest in winter (December–February). Interannually, the larger propagation velocities mostly appeared in La Niña years in the negative phases of PDO. During the eddy life span, the propagation velocities ($\boldsymbol{C}$) firstly decrease, then keep low values and finally increase in three stages of growth (20% of the life span), stable (50%) and dissipation (30%). The life-span variation of $\boldsymbol{C}$ is strongly related to the reversal variation of the rotating velocity (V_e) with R^2 of –0.93, implying energy transfer between the translation and rotating motions.

(3) Extremely slow (fast) moving eddies that slower (faster) than 1.5 cm/s (15.4 cm/s) are defined. Most SMEs occur in the central basin, more in summer and less in winter, and shift to the northern SCS in summer. In contrast, most FMEs occur at the northern and southern boundaries, less in summer and more in winter, and concentrate in the basin in autumn. The mechanism analysis shows that the background current regulates the spatiotemporal distribution of mesoscale eddy propagation velocities in the SCS.

Acknowledgements

The satellite altimeter data are downloaded from archiving validation and interpretation of satellite data in oceanography (AVISO), the Centre National d'Etudes Spatiales (CNES) of France (http://www.aviso.altimetry.fr/en/data/products/seasurface-height-products/global.html). Simple Ocean Data Assimilation (SODA v3.7.2) ocean current data are downloaded from https://www.atmos.umd.edu/~ocean/index_files/soda3.7.2_mn_download.htm. Niño 3.4 index is downloaded from https://www.esrl.noaa.gov/psd/data/correlation/nina34.data. PDO index is download from https://www.esrl.noaa.gov/psd/data/correlation/pdo.data.

References

Adams D K, McGillicuddy D J Jr, Zamudio L, et al. 2011. Surface-generated mesoscale eddies transport deep-sea products from hydrothermal vents. Science, 332(6029): 580–583, doi: 10.1126/science.1201066

Bao Ying. 2007. Primary study of the South China Sea circulation inter-annual variation (in Chinese) [dissertation]. Qingdao: Ocean University of China

Benitez-Nelson C R, Bidigare R R, Dickey T D, et al. 2007. Mesoscale eddies drive increased silica export in the subtropical Pacific Ocean. Science, 316(5827): 1017–1021, doi: 10.1126/science.1136221

Chelton D B, Schlax M G, Samelson R M. 2011. Global observations of nonlinear mesoscale eddies. Progress in Oceanography, 91(2): 167–216, doi: 10.1016/j.pocean.2011.01.002

Chen Gengxin. 2010. Mesoscale eddies in the South China Sea: Mean properties and spatio-temporal variability (in Chinese) [dissertation]. Qingdao: The Institute of Oceanology, Chinese Academy of Sciences

Chen Gengxin, Hou Yijun, Chu Xiaoqing. 2011. Mesoscale eddies in the South China Sea: Mean properties, spatiotemporal variability, and impact on thermohaline structure. Journal of Geophysical Research: Oceans, 116(C6): C06018

Cheng Xuhua, Qi Yiquan. 2008. Distribution and propagation of mesoscale eddies in the global oceans learnt from altimetric data. Advances in Marine Science (in Chinese), 26(4): 447–453

Cheng Xuhua, Qi Yiquan, Wang Weiqiang. 2005. Seasonal and interannual variabilities of mesoscale eddies in South China Sea. Journal of Tropical Oceanography (in Chinese), 24(4): 51–59

Cheng Xuhua, Xie Shangping, Du Yan, et al. 2016. Interannual-to-decadal variability and trends of sea level in the South China Sea. Climate Dynamics, 46(9–10): 3113–3126

Chow C H, Hu J H, Centurioni L R, et al. 2008. Mesoscale Dongsha cyclonic eddy in the northern South China Sea by drifter and satellite observations. Journal of Geophysical Research: Oceans, 113(C4): C04018

Chu Xiaoqing, Dong Changming, Qi Yiquan. 2017. The influence of ENSO on an oceanic eddy pair in the South China Sea. Journal of Geophysical Research: Oceans, 122(3): 1643–1652, doi: 10.1002/2016JC012642

Cui Fengjuan. 2015. Mesoscale eddies in the South China Sea: Identification and statistical characteristics analysis (in Chinese) [dissertation]. Qingdao: Ocean University of China

Frenger I, Münnich M, Gruber N. 2018. Imprint of southern ocean mesoscale eddies on chlorophyll. Biogeosciences, 15(15): 4781–4798, doi: 10.5194/bg-15-4781-2018

Hausmann U, Czaja A. 2012. The observed signature of mesoscale eddies in sea surface temperature and the associated heat transport. Deep Sea Research Part I: Oceanographic Research Papers, 70: 60–72, doi: 10.1016/j.dsr.2012.08.005

He Yinghui, Xie Jieshuo, Cai Shuqun. 2016. Interannual variability of winter eddy patterns in the eastern South China Sea. Geophysical Research Letters, 43(10): 5185–5193, doi: 10.1002/2016GL068842

He Qingyou, Zhan Haigang, Cai Shuqun, et al. 2018. A new assessment of mesoscale eddies in the South China Sea: Surface features, three-dimensional structures, and thermohaline transports. Journal of Geophysical Research: Oceans, 123(7): 4906–4929, doi: 10.1029/2018JC014054

Hu Jianyu, Kawamura H, Hong Huasheng, et al. 2000. A review on the currents in the South China Sea: Seasonal circulation, South China Sea warm current and Kuroshio intrusion. Journal of Oceanography, 56(6): 607–624, doi: 10.1023/A:1011117531252

Huang Yawen, Hua Lijuan, Zhong Linhao, et al. 2016. Characteristics of mesoscale eddies in South China Sea. Journal of University of Chinese Academy of Sciences, 33(1): 97–106

Johnson W K, Miller L A, Sutherland N E, et al. 2005. Iron transport by mesoscale Haida eddies in the Gulf of Alaska. Deep Sea Research Part II: Topical Studies in Oceanography, 52(7–8): 933–953

Li Jiaxun, Zhang Ren, Jin Baogang. 2011. Eddy characteristics in the northern South China Sea as inferred from Lagrangian drifter data. Ocean Science, 7(5): 661–669, doi: 10.5194/os-7-661-2011

Lin Pengfei. 2005. Statistical analyses on mesoscale eddies in the South China Sea and the Northwest Pacific (in Chinese) [dissertation]. Qingdao: The Institute of Oceanology, Chinese Academy of Sciences

Lin Hongyang, Hu Jianyu, Zheng Quanan. 2012a. Satellite altimeter data analysis of the South China Sea and the northwest Pacific Ocean: Statistical features of oceanic mesoscale eddies. Journal of Oceanography in Taiwan Strait (in Chinese), 31(1): 105–113

Lin Hongyang, Hu Jianyu, Zheng Quanan. 2012b. Statistical analysis of the features of meso-scale eddies near the Luzon Strait. Haiyang Xuebao (in Chinese), 34(1): 1–7

Liu Yu, Dong Changming, Guan Yuping, et al. 2012. Eddy analysis in the subtropical zonal band of the North Pacific Ocean. Deep Sea Research Part I: Oceanographic Research Papers, 68: 54–67, doi: 10.1016/j.dsr.2012.06.001

Lobel P S, Robinson A R. 1986. Transport and entrapment of fish lar-

vae by ocean mesoscale eddies and currents in Hawaiian waters. Deep Sea Research Part A. Oceanographic Research Papers, 33(4): 483–500, doi: 10.1016/0198-0149(86)90127-5
Lv Mingkun, Zang Nan, Wang Fan. 2017. Preliminary study mesoscale eddies in the Tropical Western Pacific. Marine Sciences (in Chinese), 41(10): 67
McGillicuddy D J Jr, Robinson A R, Siegel D A, et al. 1998. Influence of mesoscale eddies on new production in the Sargasso Sea. Nature, 394(6690): 263–266, doi: 10.1038/28367
Morrow R, Birol F, Griffin D, et al. 2004. Divergent pathways of cyclonic and anti-cyclonic ocean eddies. Geophysical Research Letters, 31(24): L24311, doi: 10.1029/2004GL020974
Nan Feng, Xue Huijie, Xiu Peng, et al. 2011. Oceanic eddy formation and propagation southwest of Taiwan. Journal of Geophysical Research: Oceans, 116(C12): C12045, doi: 10.1029/2011JC007386
Pilo G S, Mata M M, Azevedo J L L. 2015. Eddy surface properties and propagation at Southern Hemisphere western boundary current systems. Ocean Science, 11(4): 629–641, doi: 10.5194/os-11-629-2015
Qiu Fuwen, Fang Wendong, Zhu Dayong, et al. 2015. Characteristics and mechanism of the sea level rise in the South China Sea during 2005–2010. Journal of Tropical Oceanography (in Chinese), 34(5): 11–18
Qu Tangdong, Kim Y Y, Yaremchuk M, et al. 2004. Can Luzon Strait transport play a role in conveying the impact of ENSO to the South China Sea?. Journal of Climate, 17(18): 3644–3657, doi: 10.1175/1520-0442(2004)017<3644:CLSTPA>2.0.CO;2
Salihoğlu İ, Saydam C, Baştürk Ö, et al. 1990. Transport and distribution of nutrients and chlorophyll-*a* by mesoscale eddies in the Northeastern Mediterranean. Marine Chemistry, 29: 375–390, doi: 10.1016/0304-4203(90)90024-7
Shu Yeqiang, Chen Ju, Li Shuo, et al. 2019. Field-observation for an anticyclonic mesoscale eddy consisted of twelve gliders and sixty-two expendable probes in the northern South China Sea during summer 2017. Science China Earth Sciences, 62(2): 451–458, doi: 10.1007/s11430-018-9239-0
Shu Yeqiang, Xiu Peng, Xue Huijie, et al. 2016. Glider-observed anticyclonic eddy in northern South China Sea. Aquatic Ecosystem Health & Management, 19(3): 233–241
Tuo Pengfei, Yu Jinyi, Hu Jianyu. 2019. The changing influences of ENSO and the pacific meridional mode on mesoscale eddies in the South China Sea. Journal of Climate, 32(3): 685–700, doi: 10.1175/JCLI-D-18-0187.1
Wang Guihua, Su Jilan, Chu P C. 2003. Mesoscale eddies in the South China Sea observed with altimeter data. Geophysical Research Letters, 30(21): 2121, doi: 10.1029/2003GL018532
Wang Guihua, Su Jilan, Qi Yiquan. 2005. Advances in studying mesoscale eddies in South China Sea. Advance in Earth Sciences, 20(8): 882–886
Wang Dongxiao, Wang Qiang, Cai Shuqun, et al. 2019. Advances in research of the mid-deep South China Sea circulation. Science China Earth Sciences, 62(12): 1992–2004, doi: 10.1007/s11430-019-9546-3
Wang Chunzai, Wang Weiqiang, Wang Dongxiao, et al. 2006. Interannual variability of the South China Sea associated with El Niño. Journal of Geophysical Research Oceans, 111(C3): C03023
Wei Zexun, Zheng Quanan, Yang Yongzeng, et al. 2019. Physical oceanography research in China over past 70 years: Overview of development history and academic achievements. Haiyang Xuebao (in Chinese), 41(10): 23–64
Wu C R, Chiang T L. 2007. Mesoscale eddies in the northern South China Sea. Deep-Sea Research Part II: Topical Studies in Oceanography, 54(14–15): 1575–1588
Xie Lingling, Zheng Quanan. 2017. New insight into the South China Sea: Rossby normal modes. Acta Oceanologica Sinica, 36(7): 1–3, doi: 10.1007/s13131-017-1077-0
Xie Lingling, Zheng Quanan, Tian Jiwei, et al. 2016. Cruise observation of Rossby waves with finite wavelengths propagating from the Pacific to the South China Sea. Journal of Physical Oceanography, 46(10): 2897–2913, doi: 10.1175/JPO-D-16-0071.1
Xie Lingling, Zheng Quanan, Zhang Shuwen, et al. 2018. The Rossby normal modes in the South China Sea deep basin evidenced by satellite altimetry. International Journal of Remote Sensing, 39(2): 399–417, doi: 10.1080/01431161.2017.1384591
Xiu Peng, Chai Fei, Shi Lei, et al. 2010. A census of eddy activities in the South China Sea during 1993–2007. Journal of Geophysical Research: Oceans, 115(C3): C03012
Yang Guang, Wang Fan, Li Yuanlong, et al. 2013. Mesoscale eddies in the northwestern subtropical Pacific Ocean: Statistical characteristics and three-dimensional structures. Journal of Geophysical Research: Oceans, 118(4): 1906–1925, doi: 10.1002/jgrc.20164
Yang Guang, Yu Weidong, Yuan Yeli, et al. 2015. Characteristics, vertical structures, and heat/salt transports of mesoscale eddies in the southeastern tropical Indian Ocean. Journal of Geophysical Research: Oceans, 120(10): 6733–6750, doi: 10.1002/2015JC011130
Zhang Yu, Guan Yuping. 2019. Striations in marginal seas and the mediterranean sea. Geophysical Research Letters, 46(5): 2726–2733, doi: 10.1029/2018GL081050
Zhang Zhiwei, Tian Jiwei, Qiu Bo, et al. 2016. Observed 3D structure, generation, and dissipation of oceanic mesoscale eddies in the South China Sea. Scientific Reports, 6: 24349, doi: 10.1038/srep24349
Zhang Zhengguang, Wang Wei, Qiu Bo. 2014. Oceanic mass transport by mesoscale eddies. Science, 345(6194): 322–324, doi: 10.1126/science.1252418
Zheng Zhewen, Ho C R, Kuo N J. 2007. Mechanism of weakening of west Luzon eddy during La Nina years. Geophysical Research Letters, 34(11): L11604, doi: 10.1029/2007GL030058
Zheng Quanan, Ho Chungru, Xie Lingling, et al. 2019. A case study of a Kuroshio main path cut-off event and impacts on the South China Sea in fall-winter 2013–2014. Acta Oceanologica Sinica, 38(4): 12–19, doi: 10.1007/s13131-019-1411-9
Zheng Quanan, Hu Jianyu, Zhu Benlu, et al. 2014. Standing wave modes observed in the South China Sea deep basin. Journal of Geophysical Research: Oceans, 119(7): 4185–4199, doi: 10.1002/2014JC009957
Zheng Quanan, Tai Changkuo, Hu Jianyu, et al. 2011. Satellite altimeter observations of nonlinear Rossby eddy-Kuroshio interaction at the Luzon Strait. Journal of Oceanography, 67(4): 365–376, doi: 10.1007/s10872-011-0035-2
Zheng Quanan, Xie Lingling, Zheng Zhiwen, et al. 2017. Progress in research of mesoscale eddies in the South China Sea. Advances in Marine Science (in Chinese), 35(2): 131–158
Zu Tingting, Wang Dongxiao, Wang Qiang, et al. 2020. A revisit of the interannual variation of the South China Sea upper layer circulation in summer: Correlation between the eastward jet and northward branch. Climate Dynamics, 54(C7): 457–471